Desalination and Water Treatment
www.deswater.com

doi:10.5004/dwt.2017.0477

69 (2017) 284–293
March

Preparation of nano-Fe_2O_3 particles and evaluation of their catalytic activity in adsorption of Pb(II), Mn(II) and Zn(II) from aqueous solution

Nadia A. Youssef[a], Seham A. Shaban[b,*], Fatma A. Ibrahim[a], Amira M. Mahmoud[a]

[a]*Faculty of Girls, Ain Shams University, Cairo, Egypt, emails: nnaadd@hotmail.com (N.A. Youssef), fa_782@yahoo.com (F.A. Ibrahim), ammaahmed@yahoo.com (A.M. Mahmoud)*
[b]*Catalysts Characterization Laboratory, Catalysis department - Petroleum Refining Division, Egyptian Petroleum Research Institute (EPRI), 1 Ahmed El Zomour St., Nasr city, PO Box 11727, Cairo, Egypt, email: sehamshaban@yahoo.com*

Received 30 April 2016; Accepted 21 August 2016

ABSTRACT

Heavy metal pollution has become one of the most serious environmental problems today. The treatment of heavy metals is of special concern due to their recalcitrance and persistence in the environment. Ferric oxide nanoparticles were synthesized and were used for the removal of Pb(II), Mn(II) and Zn(II) from aqueous solution. The properties of this adsorbent were characterized by X-ray diffraction analysis, transmission electron microscopic (TEM), Fourier transform infrared spectroscopy (FTIR), the specific surface area, average particle size pore volume and pore diameter of the catalyst samples prepared were determined by N2 adsorption at –196°C. Experiments were carried out to investigate the influence of different sorption parameters, such as contact time, initial concentration of adsorbate, the concentration of Fe_2O_3 nanocatalyst and competitive adsorption behavior. It was observed that ferric oxides prepared by organic solvent method is more active than that prepared by precipitation and microwave method. The results showed that the first-order reaction law fits the reduction of metal ions, which shows good linear relationship, and the correlation coefficient (R) is larger than 0.9.

Keywords: Adsorption; Heavy metal pollution; Ferric oxide nanoparticles

1. Introduction

The contamination of wastewater and surface water by toxic heavy metals is a worldwide environmental problem. These toxic metal ions commonly exist in process waste streams from mining operations, metal plating facilities, power generation facilities, electronic device manufacturing units and tanneries. Because of economic and environmental factors, the removal and recovery of heavy-metal ions from industrial wastewater have been a significant concern in most industrial branches [1–3].

Exposure to heavy metals, even at trace level, is believed to be a risk for human beings [4–7]. Thus, how to effectively and deeply remove undesirable metals from water systems is still a very important but still challenging task for environmental engineers [8]. Nowadays, numerous methods have been proposed for efficient heavy metal removal from water, including but not limited to chemical precipitation, ion exchange, adsorption, membrane filtration and electrochemical technologies [9–14]. Among these techniques, adsorption offers flexibility in design and operation, and in many cases, it will generate high-quality treated effluent. In addition, owing to the reversible nature of most adsorption processes, the adsorbents can be regenerated by suitable desorption processes for multiple use [15], and many desorption processes are of low maintenance cost, high efficiency and ease of operation [16]. Therefore, the adsorption process is one of the major techniques for heavy metal removal from aqueous solutions [17].

*Corresponding author.

Presented at the EDS conference on Desalination for the Environment: Clean Water and Energy, Rome, Italy, 22–26 May 2016.

Among the available adsorbents, nanosized metal oxides (NMOs), including nanosized ferric oxides, manganese oxides, aluminum oxides, titanium oxides, magnesium oxides and cerium oxides, are classified as the promising ones for heavy metals removal from aqueous systems [18–20].

The both size and shape of NMOs are important factors to affect their adsorption performance.

In this paper, systematic laboratory investigations of the removal of Pb(II), Mn(II) and Zn(II) from aqueous solutions by adsorption onto Fe_2O_3 were performed.

2. Materials and methods

2.1. Adsorbate

Stock solutions of heavy metals at 1,000 mg/L concentrations were prepared by dissolving 1,000 mg of $Pb(NO_3)_2$, $MnCl_2.4H_2O$ and $ZnCl_2$ for Pb(II), Mn(II) and Zn(II) ions, respectively, in 1 L distilled water. Different solutions with concentrations from10 to100 mg/L of Pb(II), Mn(II) and Zn(II) ions were prepared by dilution using distilled water and utilized for adsorption experiments.

2.2. Adsorbent

In this work, the metal oxides were prepared by precipitation, organic solvent and microwave methods.

2.2.1. Preparation of Fe_2O_3 by precipitation method

The metal hydroxide is firstly performed by slow addition of 0.1 M NaOH to 0.1 M ferric nitrate solution (ratio 1:1) with vigorous stirring. The formed hydroxides precipitates are filtered and dried at 100°C overnight, then calcined at 400°C for 2 h in order to obtain the corresponding Fe_2O_3 catalyst (Fe_2O_3-ppt).

2.2.2. Preparation of Fe_2O_3 by organic solvent method

A slow addition of 1 M of sodium hydroxide dissolved in ethanol solution to 0.2 M of ferric nitrate (ratio 1:1) dissolved in ethanol solution with vigorous stirring. The precipitates are washed with ethanol several times until the filtrate become colorless and washing with acetone; then, they are dried at room temperature and calcined at 400°C for 1 h to obtain the corresponding Fe_2O_3 catalyst (Fe_2O_3-org).

2.2.3. Preparation of Fe_2O_3 by microwave method

The metal oxides were prepared by precipitation of metal hydroxide by slow addition of 0.1 M NaOH to 0.1 M metal nitrate solution (ratio 1:1) with vigorous stirring. The formed hydroxides precipitates are then well washed with distilled water, then irradiated by microwave (2.45 GHz, 900 W) so long as a dry powder precipitated.

2.3. Apparatus

A Philips 1390 X-ray powder diffractometer. Perkin-Elmer 2380 atomic absorption spectrometer was used for determination of Pb(II), Mn(II) and Zn(II). The flame type was air acetylene. FTIR spectra were obtained by Perkin-Elmer 1000. Quantachrome Corporation Autosorb-1-C/MS was used for BET surface area determination. The magnetic properties of the investigated solids were measured at room temperature using a vibrating sample magnetometer (VSM; 9600-1LDJ, USA) in a maximum applied field of 15 kOe. From the obtained hysteresis loops, the saturation magnetization (Ms), remanence magnetization (Mr) and coercivity (Hc) were estimated.

2.4. Adsorption experiments

Batch adsorption experiments were carried out at room temperature by shaking a series of bottles containing the desired quantity of adsorbent in a predetermined concentration of heavy metal solutions. Samples were withdrawn at different time intervals. Supernatant was separated by filtration and analyzed for remaining heavy metal content. The percentage removal of heavy metal from solution was calculated by using the following equation:

$$\% \text{ Adsorption} = \frac{C_o - C_e}{C_o} \times 100 \quad (1)$$

where C_0 is initial concentration of heavy metal; C_e is final concentration of heavy metal.

2.5. Adsorption isotherms

The studies of adsorption isotherms for the solid-liquid system are very important to realize information about adsorption capacity of adsorbents. The distribution of metal ions between the solid phase and the liquid phase can be described by several isotherm models such as the standard Langmuir isotherm model and the Freundlich isotherm model.

2.5.1. The Langmuir model

The Langmuir model isotherm assumes that the removal of metal ions occurs on a homogeneous surface by monolayer adsorption without any interaction between adsorbed ions [21]. The linearly transformed Langmuir isotherm is used to fit the adsorption data in this study and is expressed as follows:

$$\frac{1}{q_e} = \left(\frac{1}{q_m k_L}\right) \cdot \left(\frac{1}{C_e}\right) + \frac{1}{q_m} \quad (2)$$

where C_e is the equilibrium concentration of the metal ions in solution (mg/L); q_e is the amount of metal ion adsorbed on adsorbents (mg/g); and q_m and k_L are the monolayer adsorption capacity (mg/g) and the Langmuir equilibrium constant (L/mg), which indicates the nature of adsorption, respectively. The values of q_m and k_L were determined graphically. A plot of $1/q_e$ vs. $1/c_e$ gives a straight line of slope $1/q_m k_L$, and the intercept is $1/q_m$, which corresponds to complete monolayer coverage.

2.5.2. The Freundlich model

The Freundlich model isotherm assumes that the adsorption of metal ions occurs on a heterogeneous surface by monolayer adsorption. The model can be described by the following equation:

$$\log g_e = \log k_F + \frac{1}{n}\log C_e \quad (3)$$

where k_F and n are Freundlich constants [22]. The values of k_F and n were determined graphically. A plot of log q_e vs. log C_e gives a straight line of slope $\frac{1}{n}$, and the intercept is log k_F.

3. Results and discussion

3.1. Characteristics of adsorbing material (iron oxides nanoparticle)

3.1.1. X-ray diffraction (XRD)

Fig. 1 shows XRD patterns obtained from Fe-ppt, Fe-org and Fe-mic nanoparticles samples. Amorphous behavior of Fe-org and Fe-mic nanoparticles are showed in the XRD patterns with no significant diffraction peaks. For Fe-ppt nanoparticles, there were some weak peaks vaguely appeared at 30.42° and 35.70°, which were assigned to the (206) and (313) diffraction planes of the γ-Fe_2O_3 phase [23].

3.1.2. FTIR analysis

The FTIR spectra of the ferric oxides prepared by precipitation, organic solvent and microwave methods are shown in Fig. 2; the intensity of a broad peak at about 3,400 cm^{-1} corresponds to H-OH stretch reduces with annealing temperature, which may be explained by evaporation of moieties in the samples. The absorption bands in the range 400–750 cm^{-1}, which are characterized for the Fe-O vibration mode, are present in all samples [22,23]. The FTIR spectrum of samples shows two broad bands at 3,455 and 3,144 cm^{-1}. The band at 3,455 cm^{-1} can be assigned to the stretching modes of surface H_2O molecules or to an envelope of hydrogen-bonded surface OH groups. The band at 3,144 cm^{-1} can be assigned to the OH stretching mode in the goethite structure. The band at 1,643 cm^{-1} is close to the position of H_2O bending vibrations. Two bands at 895 and 798 cm^{-1} are due to Fe-O-H bending vibrations in goethite; the IR band at 624 cm^{-1} can be assigned to Fe-O stretching vibration [24].

3.1.3. Transmission electron microscopic (TEM)

Fig. 3 shows the TEM images of the synthesized Fe_2O_3 nanoparticles. The images show that Fe_2O_3 nanoparticles have sizes in the range of 2–40 nm. Fig. 3(a) shows that Fe_2O_3 nanoparticles prepared by precipitation method have rod like morphologies with an average particle diameter of 17.0 nm (range 13.7–20.0 nm). Fig. 3(b) shows the image of Fe_2O_3 nanoparticles prepared by organic solvent method, which has revealed evidence that the particles exhibited morphologies with minor particles agglomeration with the average particle diameter of 1.5 nm (range 1–3 nm). The TEM image of the sample prepared by microwave method is shown in Fig. 3(c); the particles are very fine with sizes <10 nm. It is evident from the images that the particles are poorly crystalline and agglomerated [25,26].

3.1.4. Surface area measurement (BET)

Fig. 4(a) shows the N_2 adsorption–desorption isotherms, which are close to Type H4 of The International Union of Pure and Applied Chemistry (IUPAC) classification with an

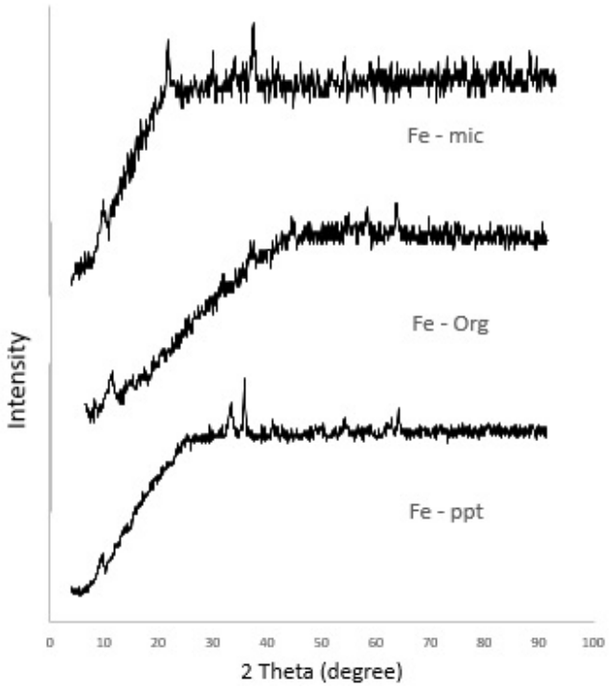

Fig. 1. X-ray diffraction of ferric oxide prepared by different methods.

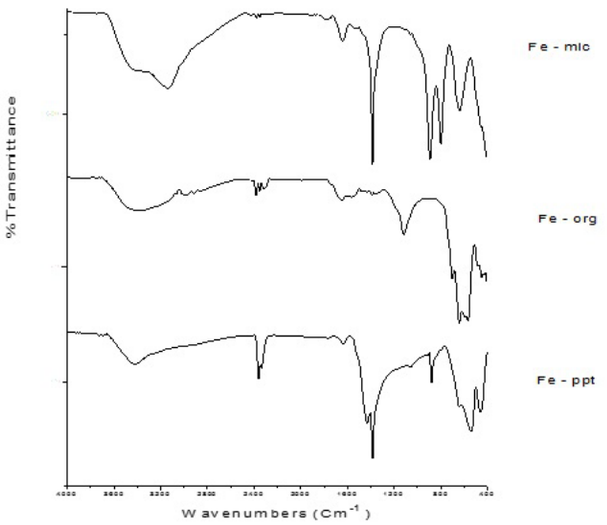

Fig. 2. FTIR spectra of ferric oxide prepared by different methods.

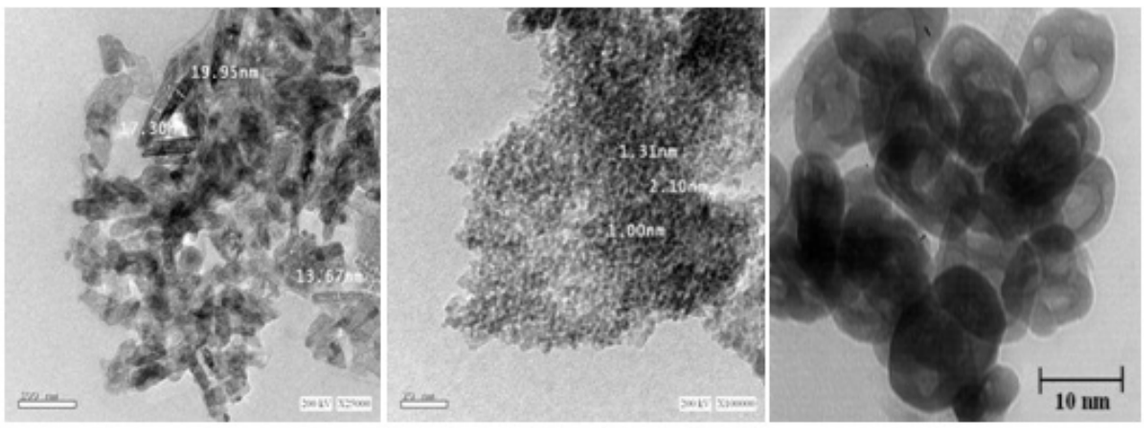

Fig. 3. TEM images for Fe_2O_3 nanoparticles prepared by: (a) precipitation, (b) organic solvent and (c) microwave methods.

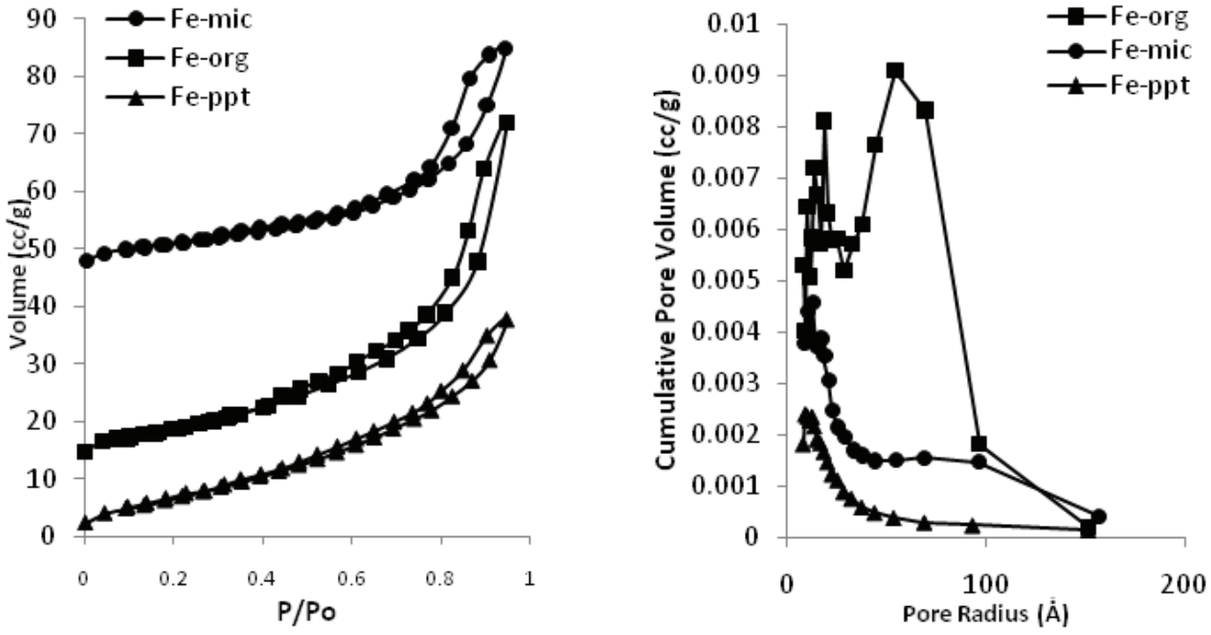

Fig. 4. Texture properties for Fe_2O_3 nanoparticles prepared by: (a) N2 adsorption-desorption isotherms, (b) pore size distribution.

evident hysteresis loop in the 0.4–1.0 range, suggesting that the sample under study is basically microporous. The specific surface areas of the samples are calculated by the BET method, and the results are illustrated in Table 1. The relatively high specific surface area of the products is related to the nanometric size of its particles. More detailed information on the porosity is available from the pore volume d istribution curves as shown in Fig. 4(b); this is constructed by plotting dv/dr against the mean pore radius [27]. It is shown from this figure that the investigated solids exhibited different models of distribution in which most of the pores were located in the micropore range. However, the maxima of the pore distribution curves were located at range of 40.7–60.28 A° (4.7–6.2 nm); the heights of these distribution curves are decreased parallels with the increase in surface area.

3.1.5. Magnetic properties

The magnetic properties of the as-prepared powders were characterized by measuring the magnetic hysteresis loop at room temperature. The obtained hysteresis loops of all the samples are shown in Fig. 5. From these measurements, the magnetic moment and the Hc are derived and listed in Table 2.

Table 1
Textural parameters of ferric oxides nanoparticles as prepared by precipitation, organic solvent and microwave methods

Metal oxides	S_{BET} (m^2/g)	*Vp* (ml/g)	*r′* (Å)
Fe-org	50.46	0.096	40.7
Fe-mic	31.71	0.125	49.63
Fe-ppt	28.78	0.059	60.28

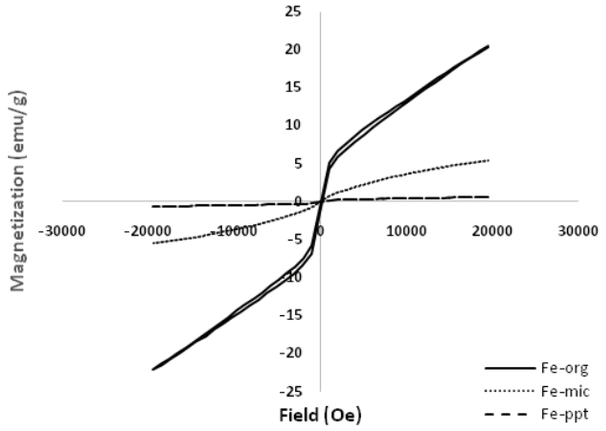

Fig. 5. The magnetic properties of the prepared iron nanoparticle.

Table 2
The magnetic properties (Ms, Mr and Hc) of the as-prepared iron nanoparticle

	Fe-org	Fe-mic	Fe-ppt
Coercivity (Hc), G	115.31	50.797	34.489
Magnetization (Ms), emu/g	2.3789	0.65259	0.021265
Retentivity (Mr), emu/g	0.11177	0.012073	0.00064348

It was found that the Hc decreased as the particle size decreased; also, the magnitude of the Ms decreased as the particle size decreased. It is found that the increasing tendency of Ms, Mr and Hc are consistent with the improvement of crystallinity. However, the Ms of γ-Fe_2O_3 nanocrystallites is significantly lower than that of bulk γ-Fe_2O_3 (2.37 emu/g) [28,29], which can probably be attributed to the nanoscale dimension and the surface defects [30–32].

The Ms obtained for Fe-Org was found to be 2.3789 emu/g, and remnant magnetization (Mr) was 0.11177 emu/g, Table (2). It was found that the iron prepared by organic method exhibited an Ms greater than that of iron prepared by microwave and precipitation methods [33].

3.2. Removal of heavy metal ions from aqueous solutions

3.2.1. Effect of contact time on heavy metal removal by ferric oxides

The results obtained for adsorptive removal of Pb(II), Mn(II) and Zn(II) with respect to the contact time are shown in Fig. 6. The removal percentage of Pb(II) increases gradually from 63.14% to 99.82% for Fe-ppt, from 95.20% to 100.00% for Fe-org and from 93.18% to 99.86% for Fe-mic with increasing contact time from 10 to 240 min, respectively. The adsorption of Mn(II) increases gradually from 35.20% to 61.40% for Fe-ppt, from 79.40% to 99.76% for Fe-org and from 68.12% to 80.40% for Fe-mic by increasing the contact time from 10 to 240 min, respectively. The adsorption of Zn(II) increases gradually from 77.00% to 99.14% for Fe-ppt, from 99.62% to 100.00% for Fe-org and from 90.00% to 99.86% for Fe-mic by increasing the contact time from 10 to 240 min, respectively.

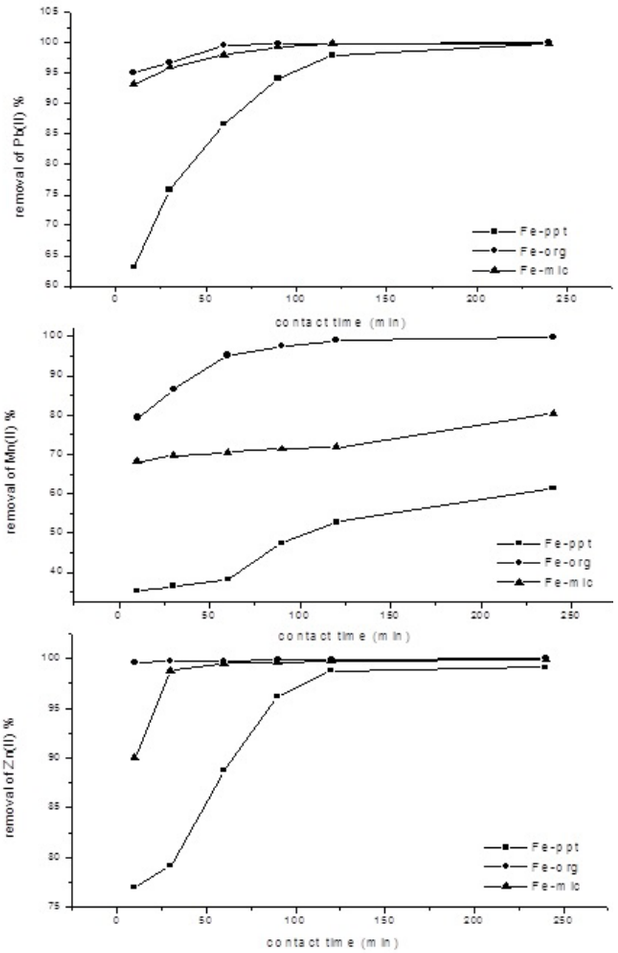

Fig. 6. Effect of contact time on the removal percentage of Pb(II), Mn(II) and Zn(II) by ferric oxides, temperature 298 K.

3.2.2. Effect of the weight of ferric oxides on heavy metal removal

The results obtained for adsorptive removal of Pb(II), Mn(II) and Zn(II) with respect to the adsorbent quantity are shown in Fig. 7. From this figure, it is shown that the removal percentage of Pb(II) has increased gradually from 97.94% to 99.64% for Fe-ppt, from 99.86% to 100% for Fe-org and from 99.82% to 100% for Fe-mic with increasing Fe_2O_3

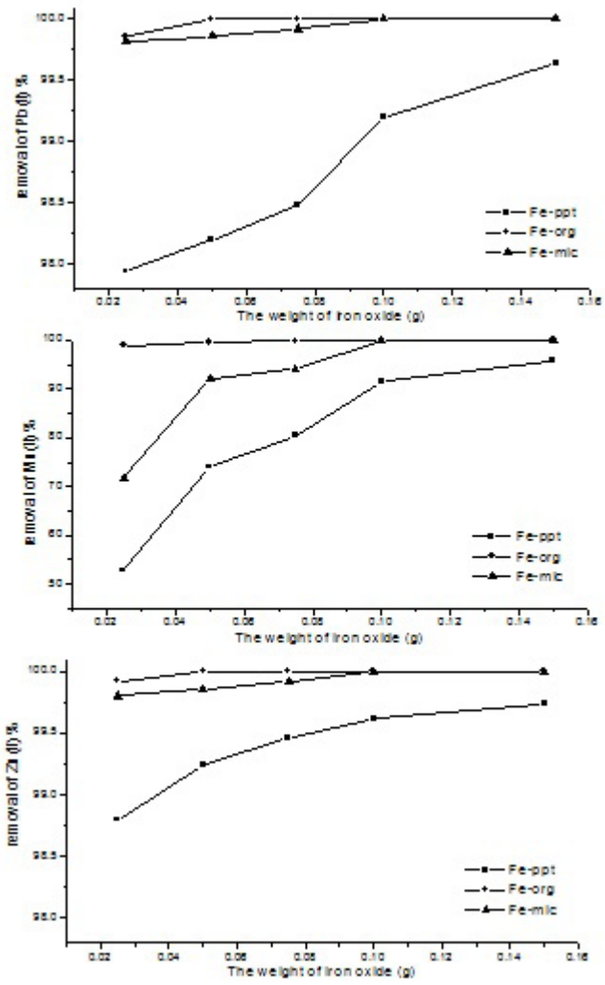

Fig. 7. Effect of the weight of ferric oxides on the removal percentage of Pb(II), Mn(II) and Zn(II) (contact time 120 min, temperature 298 K).

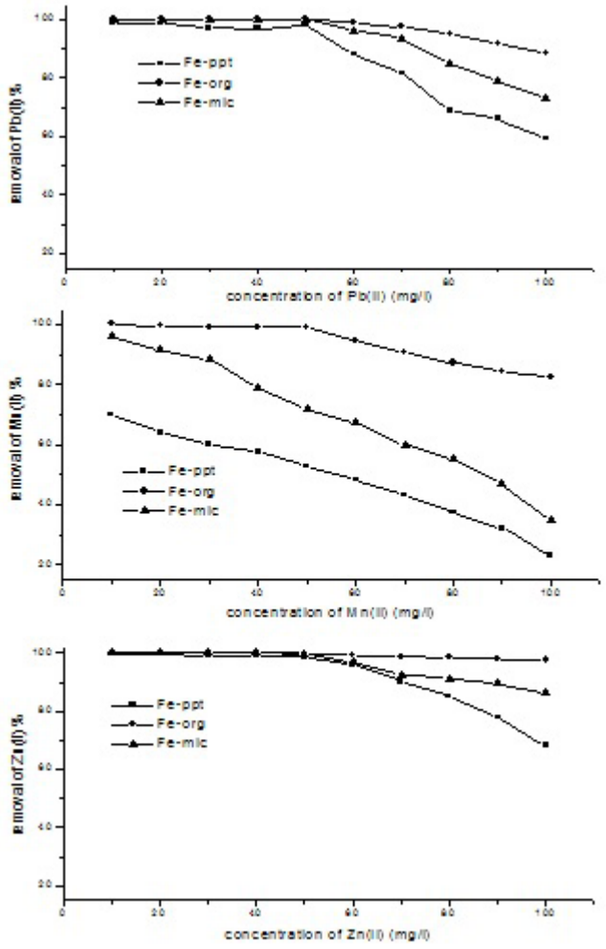

Fig. 8. Effect of the variation of initial concentration of Pb(II), Mn(II) and Zn(II) on the removal percentage of Pb(II), Mn(II) and Zn(II) by ferric oxides (contact time 120 min, temperature 298 K).

quantity from 0.025 to 0.150 g, respectively. The adsorption of Mn(II) increases gradually from 52.78% to 96% for Fe-ppt, from 98.96% to 100% for Fe-org and from 71.80% to 100% for Fe-mic with increasing amount of ferric oxides from 0.025 to 0.150 g, respectively. It was observed that the adsorption of Zn(II) increases gradually from 98.80% to 99.74% for Fe-ppt, from 99.92% to 100% for Fe-org and from 90.80% to 100% for Fe-mic with increasing amount of ferric oxides from 0.025 to 0.150 g, respectively.

3.2.3. Effect of the variation of the initial heavy metal concentration

Fig. 8 shows the percentage of removal of Pb(II), Mn(II) and Zn(II) by ferric oxide. It was observed that the adsorption decreases gradually from 98.80% to 59.21% for Fe-ppt, from 100% to 88.30% for Fe-org and from 100% to 73% for Fe-mic with the increase in the initial lead concentration from 10 to 100 mg/L, respectively. The adsorption decreases gradually from 70% to 23% for Fe-Ppt, from 100% to 82.20% for Fe-org and from 96% to 35% for Fe-mic with increasing in initial manganese concentration from 10 to 100 mg/L, respectively. It was found that the adsorption of Zn(II) decreases gradually from 99.60% to 68.10% for Fe-ppt, from 100% to 97.60% for Fe-org and from 100% to 86.10% for Fe-mic with increasing in initial zinc concentration from 10 to 100 mg/L, respectively.

From Fig. 6, the removal percentage of Pb(II), Mn(II) and Zn(II) increases with increasing contact time and attained saturation (equilibrium time) in about 120 min. Basically, the rate of removal of these adsorbates is rapid during the first 30 min due to the larger surface area and active sites of the adsorbent being available for the adsorption of the metals; then, the removal percentage becomes almost insignificant due to a quick exhaustion of adsorption sites.

From Fig. 7, the adsorption was found to be increased with increasing weight of ferric oxides up to a certain limit and then became almost constant due to the increasing surface area and active sites.

From Fig. 8, it can be concluded that at lower initial concentration of metal ions, sufficient adsorption sites may be available for adsorption of heavy metal ions but at higher concentration of metal ions their number might be greater than the number of adsorption sites and consequently less adsorption was detected [34].

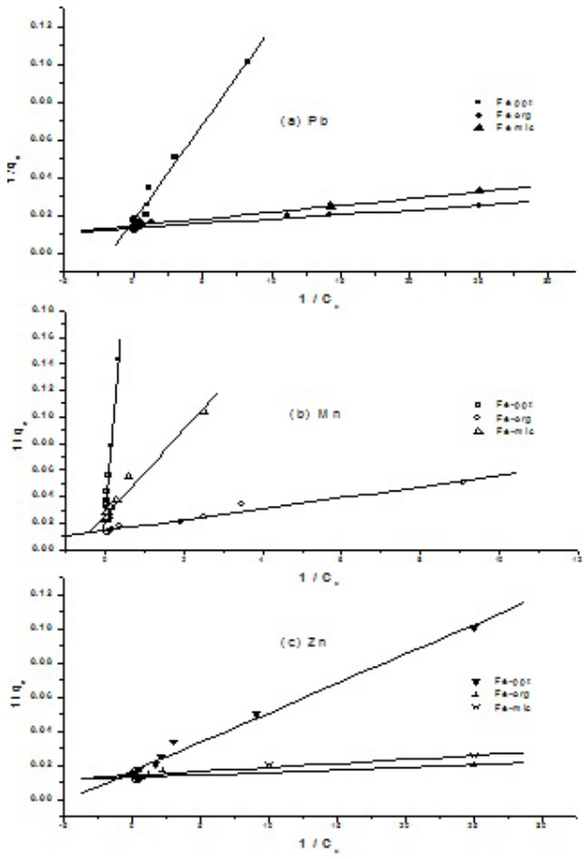

Fig. 9. Langmuir isotherms plot for removal of Pb(II), Mn(II) and Zn(II) by ferric oxides prepared by different methods.

From the above data, the removal percentage of Pb(II) > Zn(II) > Mn(II) and the best metal oxide Fe-org < Fe-mic < Fe-ppt.

3.2.4. Removal of mixed heavy metal ions from aqueous solutions

When mixed three heavy metal ions [Pb(II), Mn(II) and Zn(II)] with the same concentration 30 mg/l and using 0.025 gm of Fe-org for 120 min, the removal percentage of Pb(II) is 100%, for Mn(II) is70.16% and for Zn(II) is 98.95%.

From this, the removal percentage of Pb(II) > Zn(II) > Mn(II) and that is similar to the result obtained from each heavy metal alone.

3.3. Adsorption isotherms

3.3.1. The Langmuir model

Table 2 shows the adsorption capacity, Langmuir constant and regression coefficients (R). The linear plots of $1/q_e$ against $1/c_e$ show that the adsorption obeys the Langmuir model in Fig. 9.

3.3.2. The Freundlich model

Table 3 shows Freundlich constants and regression coefficients (R). The logarithmic plot of the Freundlich expression for the amount of heavy metal ions adsorbed per unit mass of the adsorbent (q_e) and the concentration of heavy metal ions at equilibrium (C_e) is shown in Fig. 10.

The linear forms of Langmuir and Freundlich are shown graphically in Figs. 9 and 10. The regression coefficients (R) obtained from Langmuir model were much higher than those obtained from Freundlich model; therefore, the Langmuir model is better than Freundlich model and could explain the studied adsorption procedure. When the adsorption capacities of Fe-ppt, Fe-org and Fe-mic were compared for Pb(II), Mn(II) and Zn(II), it was found that Fe-org have maximum adsorption capacity for Pb(II), Mn(II)and Zn(II) obtained from Langmuir model are 74.74, 38.88 and 78.66 mg/g, respectively.

Table 3
Isotherm constants of the Langmuir and Freundlich models and regression coefficients for Pb(II), Mn(II) and Zn(II)removal by ferric oxides prepared by different methods

Metal ion	Adsorbents	Langmuir constants			Freundlich constants		
		q_m	K_L	R	K_F	n	R
Pb(II)	Fe-ppt	59.56	1.638	0.9929	28.65	3.91	0.8738
	Fe-org	74.74	28.420	0.9546	63.70	7.96	0.92621
	Fe-mic	68.68	20.320	0.9790	52.90	9.02	0.93211
Mn(II)	Fe-ppt	24.22	9.956	0.9819	5.83	2.42	0.89406
	Fe-org	38.88	0.890	0.9854	42.98	4.23	0.9177
	Fe-mic	36.68	0.081	0.9907	15.58	3.62	0.9362
Zn(II)	Fe-ppt	61.09	4.770	0.9973	37.13	3.89	0.91154
	Fe-org	78.66	42.506	0.8109	76.46	6.48	0.80154
	Fe-mic	70.78	31.419	0.9169	59.12	8.91	0.90805

Table 4
First and second orders kinetic parameters for the removal of Pb(II) Mn(II) and Zn(II) by ferric oxides

Metal ion	Adsorbents	First order			Second order		
		K_1	q_e	R	K_2	q_e	R
Pb(II)	Fe-ppt	0.026553	27.040828	0.99156	0.00210368	51.86721	0.99967
	Fe-org	0.034982	2.94089	0.94558	0.032195	50.15045	1.00000
	Fe-mic	0.044332	7.72645	0.96451	0.019051	50.175614	0.99999
Mn(II)	Fe-ppt	0.010179	16.79770	0.94429	0.0011138	33.12355	0.98885
	Fe-org	0.029639	14.523122	0.99825	0.005314	50.70993	0.99995
	Fe-mic	0.003109	6.059126	0.96976	0.003229	40.567951	0.99773
Zn(II)	Fe-ppt	0.037308	27.22826	0.95034	0.003254	50.916496	0.99959
	Fe-org	0.013288	0.20728	0.9919	0.203877	50.02501	1.00000
	Fe-mic	0.041154	3.432574	0.94923	0.032207	50.1002	0.99999

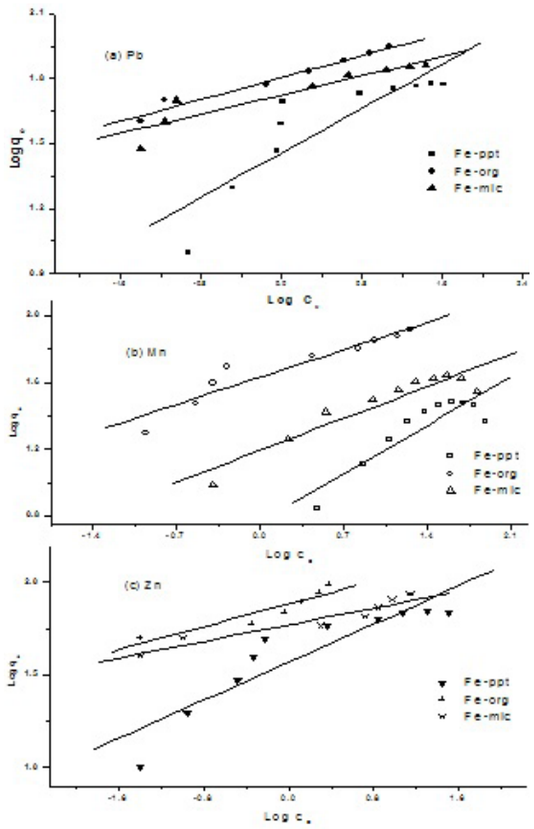

Fig. 10. Freundlich isotherms plot for removal of Pb(II), Mn(II) and Zn(II) by ferric oxides prepared by different methods.

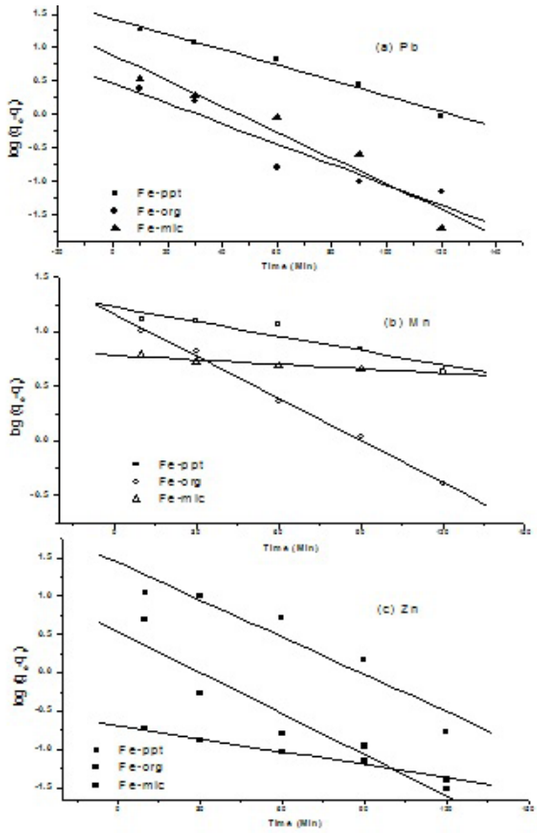

Fig. 11. First-order plots for adsorption of Pb(II)), Mn(II) and Zn(II) by ferric oxides prepared by different methods.

3.4. Adsorption kinetics

The two adsorption kinetic models used in this study are first-order and second-order equations developed by Ho and Cuevas-Villanueva et al., respectively [35,36].

The first-order equation is expressed as follows (Eq. (4)):

$$\log(q_e - q_t) = \log q_e - k_{1st}\frac{t}{2.303} \tag{4}$$

The second-order equation is expressed as follows (Eq. (5)):

$$\frac{t}{q_t} = \frac{1}{K_{2nd}q^2{}_e} + \frac{t}{q_e} \tag{5}$$

where k_{1st} and k_{2nd} are the rate constant of first-order and second-order adsorption, respectively; q_e and q_t denote the amount of adsorption at equilibrium and at time t, respectively.

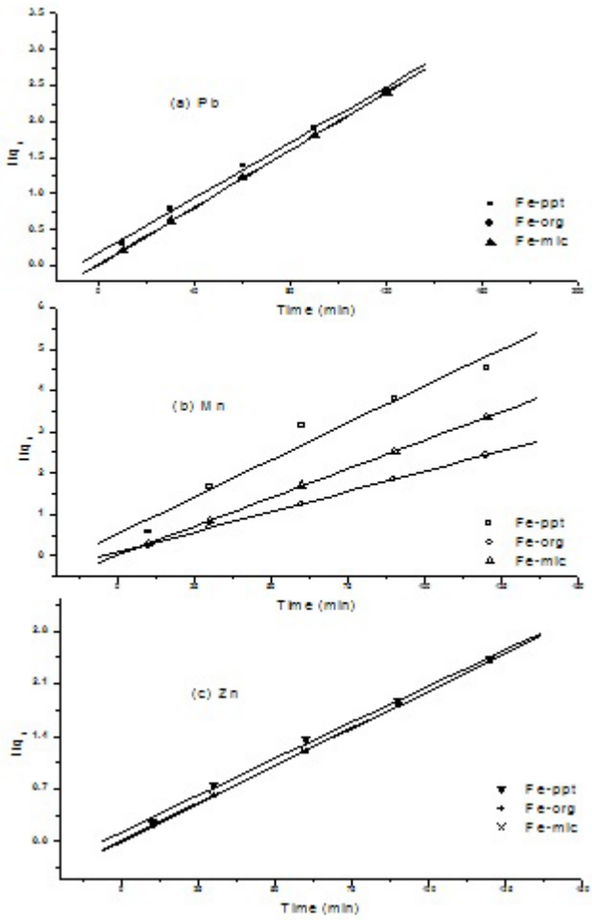

Fig. 12. Second-order plots for adsorption of Pb(II), Mn(II) and Zn(II) by ferric oxides prepared by different methods.

Kinetic parameters of these models were calculated from the slope and the intercept of the linear plots of log $(q_e - q_t)$ vs. t for first-order kinetic model and t/q_t vs. t for second-order kinetic.

The linear plots obtained for the first-order and second-order equation are shown graphically in Figs. 11 and 12. It was found from values of regression coefficients that the fit is better with second-order equation than with first-order equation. Therefore, the kinetics of heavy metals adsorption by the adsorbent can be described well by second-order equation, i.e., the adsorption process of heavy metals as adsorbates on ferric oxides nanoparticles as adsorbents can be interpreted well using the second-order equation.

4. Conclusions

The present study shows that ferric oxide-nanoparticles prepared by the organic solvent method is more active than that prepared by the precipitation and microwave methods for removal of Pb(II), Mn(II) and Zn(II) ions from aqueous solutions. The adsorption process is a function of the adsorbent and adsorbate concentrations and contact time. Equilibrium was achieved practically in 2 h. Langmuir model is found to be in a good agreement with experimental data on adaptive behavior of Pb(II), Mn(II) and Zn(II) ions on Fe_2O_3. Ferric oxide is then considered as a useful catalyst for the treatment of wastewater containing lead, manganese and zinc.

References

[1] A.F. Ngomsik, A. Bee, J.M. Siaugue, D. Talbot, V. Cabuil, G. Cote, Co(II) removal by magnetic alginate beads containing Cyanex 272, J. Hazard. Mater., 166 (2009) 1043–1049.
[2] P. Yin, Q. Xu, R. Qu, G. Zhao, Y. Sun, Adsorption of transition metal ions from aqueous solutions onto a novel silica gel matrix inorganic–organic composite material, J. Hazard. Mater., 173 (2010) 710–716.
[3] A.F. El-Kafrawy, S.M. El-Saeed, R.K. Farag, H.Al-A. El-Saied, M.El-S. Abdel-Raouf, Adsorbents based on natural polymers for removal of some heavy metals from aqueous solution, Article In Press, Accepted 18 February 2016, Available online 22 March 2016.
[4] M. Jamil, M.S. Zia, M. Qasim, Contamination of agro-ecosystem and human health hazards from wastewater used for irrigation, J. Chem. Soc. Pak., 32 (2010) 370–378.
[5] S. Khan, Q. Cao, Y.M. Zheng, Y.Z. Huang, Y.G. Zhu, Health risks of heavy metals in contaminated soils and food crops irrigated with wastewater in Beijing, China, Environ. Pollut., 152 (2008) 686–692.
[6] A. Singh, R.K. Sharma, M. Agrawal, F.M. Marshall, Health risk assessment of heavy metals via dietary intake of foodstuffs from the wastewater irrigated site of a dry tropical area of India, Food Chem. Toxicol., 48 (2010) 611–619.
[7] S.H. Peng, W.X. Wang, X.D. Li, Y.F. Yen, Metal partitioning in estuarine sediments measured by sequential extraction and biomimetic approaches, Chemosphere, 57 (2004) 839–851.
[8] M. Eloussaief, W. Hamza, N. Kallel, M. Benzina, Wastewaters decontamination: mechanisms of Pb(II), Zn(II) and Cd(II) competitive adsorption on Tunisian smectite in single and mutlisolute systems, Environ. Prog. Sustain. Energy, 32 (2013) 229–238.
[9] Guidelines for Drinking-Water Quality, 3rd ed., Vol. 1, Recommendation World Health Organization, Geneva, 2004.
[10] F.L. Fu, Q. Wang, Removal of heavy metal ions from wastewaters: a review, J. Environ. Manage., 92 (2011) 407–418.
[11] Y.H. Wang, S.H. Lin, R.S. Juang, Removal of heavy metal ions from aqueous solutions using various low-cost adsorbents, J. Hazard. Mater., 102 (2003) 291–302.
[12] D.W. O'Connell, C. Birkinshaw, T.F. O'Dwyer, Heavy metal adsorbents prepared from the modification of cellulose: a review, Bioresour. Technol., 99 (2008) 6709–6724.
[13] N. Moayyeri, K. Saeb, E. Biazar, Removal of heavy metals (lead, cadmium, zinc, nickel and iron) from water by bio-ceramic absorbers of hydroxy-apatite microparticle, Int. J. Mar. Sci. Eng., 3 (2013)13–16.
[14] Y.A. El-Taweel, E.M. Nassef, I. Elkheriany, D. Sayed, Removal of Cr(VI) ions from waste water by electrocoagulation using iron electrode, Egypt. J. Petroleum, 24 (2015) 27–35
[15] M. Hua, S. Zhang, B. Pan, W. Zhang, L. Lv, Q. Zhang, Heavy metal removal from water/wastewater by nanosized metal oxides: a review, J. Hazard. Mater., 211–212 (2012) 317–331.
[16] R.K. Gautam, A. Mudhoo, G. Lofrano, M.C. Chattopadhyaya, Biomass-derived biosorbents for metal ions sequestration: adsorbent modification and activation methods and adsorbent regeneration, J. Environ. Chem. Eng., 2 (2014) 239–259.
[17] M. Eloussaief, I. Jarraya, M. Benzina, Adsorption of copper ions on two clays from Tunisia: pH and temperature effects, Appl. Clay Sci., 46 (2009) 409–413.
[18] B.J. Pan, B.C. Pan, W.M. Zhang, L. Lv, Q.X. Zhang, S.R. Zheng, Development of polymeric and polymer-based hybrid adsorbents for pollutants removal from waters, J. Chem. Eng., 151 (2009) 19–29.
[19] B. Chen, Z. Zhu, S. Liu, J. Hong, J. Ma, Y. Qiu, J. Chen, Facile hydrothermal synthesis of nanostructured hollow iron–cerium alkoxides and their superior arsenic adsorption performance, ACS Appl. Mater. Interfaces, 6 (2014) 14016–14025.

[20] A.M. Mahmoud, F.A. Ibrahim, S.A. Shaban, N.A. Youssef, Adsorption of heavy metal ion from aqueous solution by nickel oxide nano catalyst prepared by different methods, Egypt. J. Petroleum, 24 (2015) 27–35.
[21] I. Langmuir, The adsorption of gases on plane surfaces of glass, mica and platinum, J. Am. Chem. Soc., 40 (1918) 1361–1403.
[22] Z.P. Gaoa, Z.F. Yu, T.L. Yue, S.Y. Quek, Adsorption isotherm, thermodynamics and kinetics studies of polyphenols separation from kiwifruit juice using adsorbent resin, J. Food Engng., 116(1) (2013) 195–201.
[23] N.D. Phu, D.T. Ngo, L.H. Hoang, N.H. Luong, N.H. Hai, Crystallization process and magnetic properties of amorphous iron oxide nanoparticles, J. Phys. D: Appl. Phys., 44-345002(34) (2011).
[24] G. Marijan, M. Svetozar, FT-IR and SEM investigation of iron oxides precipitated from $FeSO_4$ solutions, J. Mol. Struct., Volumes 834–836 (2007) 445–453.
[25] K.A. Avnish, S. Mohan, K. Ritu, S.J. Vivek, K. Pankaj, Synthesis, characterization, and magnetic studies of Fe_2O_3 nanoparticles, J. Nanotechnol., Article ID 474909 (2014) 1–7.
[26] R. Miss, A simple and effective method of the synthesis of nanosized Fe_2O_3 particles, IOSR J. Appl. Chem., 4 (2013) 41–46.
[27] S. Brunauer, L.S. Deming, W.E. Deming, E. Teller, On a Theory of the van der Waals adsorption of gases, J. Am. Chem. Soc., 62 (1940) 1723–1732.
[28] S. Klotz, G. Steinle-Neumann, T. Strassle, J. Philippe, T. Hansen, M.J. Wenzel, Magnetism and the Verwey transition in Fe_3O_4 under pressure, Phys. Rev. B, 77(012411)(2008) 1–4.
[29] Z.-H. Jing, S.-H. Wu, Synthesis, characterization and magnetic properties of γ-Fe_2O_3 nanoparticles via a non-aqueous medium, J. Solid State Chem., 177 (2004) 1213–1218.
[30] B. Hong, C. Qianwang, S. Tao, Preparation of ferromagnetic γ-Fe_2O_3 nanocrystallites by oxidative co-decomposition of PEG 6000 and ferrocene, Solid State Commun., 141 (2007) 573–576.
[31] R. Zboril, L. Machala, M. Mashlan, V. Sharma, Iron(III) oxide nanoparticles in the thermally induced oxidative decomposition of Prussian blue, $Fe_4[Fe(CN)6]_3$, Cryst. Growth Des., 4 (2004) 1317–1325.
[32] C.J. Serna, F. Bődker, S. Mőrup, M.P. Morales, F. Sandiumenge, S. Veintemillas-Verdaguer, Spin frustration in maghemite nanoparticles, Solid State Commun., 118 (2001) 437–440.
[33] N.M. Deraz, S. Shaban, Optimization of catalytic, surface and magnetic properties of nanocrystalline manganese ferrite, J. Anal. Appl. Pyrolysis, 86 (2009) 173–179.
[34] S.E. Bailey, T.J. Olin, R.M. Bricka, D.D. Adrian, A review of potentially low-cost sorbents for heavy metals, Water Res., 33 (1999) 2469–2479.
[35] Y.-S. Ho, Review of second-order models for adsorption systems, J. Hazard. Mater., 136 (2006) 681–689.
[36] R.A.-Cuevas-Villanueva, A.R. Hidalgo-Vázquez, C. de Jesús Cortés Penagos, R. Cortés-Martínez, Thermodynamic, kinetic, and equilibrium parameters for the removal of lead and cadmium from aqueous solutions with calcium alginate beads, Scientific. World J., Volume 2014, Article ID 647512 (2014) 1–9